Space Weather

RESEARCH ARTICLE
10.1029/2024SW004226

Satellite Internal Charging for a Reasonable Worst-Case

R. B. Horne[1], P. Y. Lam[1], N. P. Meredith[1], S. A. Glauert[1], and P. Kirsch[1]

[1]British Antarctic Survey, Cambridge, UK

Abstract Increases in the flux of high energy electrons in the Earth's radiation belts cause satellite charging which can lead to an electrostatic discharge, anomalies and disruption to service. For geostationary orbit (GEO) there are guidelines on how much shielding to protect electronic components, but not for lower orbits. Here we use data from GPS satellite NS41, the AE9 radiation model, and LANL satellite data to create a reasonable worst-case electron flux spectrum between 60 keV and 8 MeV. We calculate the charging currents for satellites in circular equatorial orbit between 4.25 and 7.0 Re and show that the recommended guideline of 2.8 mm (110 mil) of Al shielding is sufficient to keep charging below recommended guidelines at GEO. Approximately 4.5 mm (177 mil) of Al shielding would be needed for satellites in circular equatorial orbit at 4.5 Re. We show that the maximum electric field could exceed the breakdown field in cables and dielectrics just under the spacecraft surface on a timescale of 1–2 hr presenting a risk of anomalies. Radiation induced conductivity reduces the risk but is highly uncertain. A magnetic storm, series of storms or high speed stream accompanied by a large solar energetic particle event would present a much higher risk of anomalies on several satellites.

Plain Language Summary During space weather events the level of high energy charged particles (electrons) can increase substantially in regions where satellites orbit the Earth. These charged particles accumulate on satellite surfaces and internal components and can lead to an electrostatic discharge, anomalies and service disruption. Whilst there are guidelines for shielding sensitive components for satellites in geostationary orbit (GEO), there are little or no guidelines for lower orbits. In this study, data from the GPS satellite NS41, the AE9 radiation model and other satellites have been used to establish a reasonable worst-case scenario at different orbits. The analysis shows that roughly 2.8 mm (110 mil) of Aluminum shielding is enough to protect satellites in GEO from excessive charging, in agreement with existing guidelines. However, satellites in lower circular equatorial orbits (around 4.5 Earth radii) would need about 4.5 mm (177 mil). During a severe space weather event, electric fields in the insulating layers of certain cables could exceed safe levels, leading to an increased risk of anomalies. Although charged particles increase the conductivity of insulating materials and helps mitigate the risk, the effectiveness is uncertain. A severe space weather event would significantly increase the chance of anomalies on satellites without adequate protection.

Key Points:

- We construct a reasonable worst-case electron flux spectrum to calculate satellite charging
- We find that the recommended guideline of 2.8 mm of Al shielding is sufficient for geostationary orbit, but 4.5 mm is needed at 4.5 Re
- The maximum electric field in cables and dielectrics just under the satellite surface could exceed the breakdown field

Correspondence to:
R. B. Horne,
rh@bas.ac.uk

Citation:
Horne, R. B., Lam, P. Y., Meredith, N. P., Glauert, S. A., & Kirsch, P. (2025). Satellite internal charging for a reasonable worst-case. *Space Weather*, *23*, e2024SW004226. https://doi.org/10.1029/2024SW004226

Received 23 OCT 2024
Accepted 29 MAY 2025

Author Contributions:
Conceptualization: R. B. Horne
Data curation: P. Kirsch
Formal analysis: P. Y. Lam, N. P. Meredith
Funding acquisition: R. B. Horne
Investigation: R. B. Horne
Methodology: R. B. Horne, P. Y. Lam, S. A. Glauert
Project administration: R. B. Horne
Resources: P. Y. Lam
Software: P. Y. Lam, N. P. Meredith, P. Kirsch
Supervision: R. B. Horne, P. Kirsch
Validation: P. Y. Lam, N. P. Meredith
Visualization: P. Y. Lam
Writing – original draft: R. B. Horne, P. Y. Lam
Writing – review & editing: R. B. Horne, P. Y. Lam, N. P. Meredith, S. A. Glauert, P. Kirsch

1. Introduction

Satellite charging is one of the most important hazards to satellites on orbit. Charging can result in an electric discharge, damage to electronic components and phantom commands, leading to anomalies, unexpected satellite behavior and disruption to service (Baker et al., 1998; Gubby & Evans, 2002; Horne et al., 2021; Wrenn, 1995). In unusual cases it has also been responsible for the total loss of a satellite leading to loss of revenue, expensive insurance claims and early replacement costs.

Satellite charging is usually divided into surface charging and internal charging (Hastings & Garrett, 2004). Surface charging is associated with the variability of electrons with energies less than about 50 keV or so which are absorbed in the surface layers of the spacecraft. Internal charging is associated with higher energy electrons up to several MeV that are absorbed deep inside the spacecraft by dielectrics, ungrounded conductors and other materials (NASA, 2022). However, there is no clear energy separation and it is important to consider changes over the entire energy spectrum. Internal charging is also known as deep dielectric charging or bulk charging.

Surface charging usually occurs between midnight and dawn for satellites in geosynchronous orbit (GEO) due to electron injections during substorms (Choi et al., 2011; Fennell et al., 2001). Entry into and out of eclipse is also particularly important due to the change in sunlight, which affects mechanisms for ridding excess charges such as photo-electron emission. Differential charging occurs between surfaces with different voltages, and is the main cause for most surface-charging anomalies (NASA, 2022). In low Earth Orbit (LEO) surface charging usually

occurs in the pre-midnight sector (Anderson, 2012) in conjunction with electrons that are accelerated downward (i.e., upward field aligned currents) that are responsible for the aurora. Satellite charging in the topside ionosphere is associated with low background plasma density, which corresponds to a larger Debye length.

The largest risk of internal charging is from high energy electrons trapped in the Van Allen radiation belts. Statistical studies show that an increase in the >2 MeV electron flux is associated with anomalies (Gubby & Evans, 2002; Han et al., 2005; Iucci et al., 2005). The radiation belts are not static with time; they vary in location and with geomagnetic activity significantly. For example, during the 2003 Halloween storm the outer radiation belt was depleted and reformed much closer to the Earth (Baker et al., 2004; Horne, Thorne, Shprits, et al., 2005). The same thing happened in the recent storm of 10–12 May 2024 (see the link to the SaRIF web site given in the data section). In the slot region where the flux is usually very low the flux increased by over 4 orders of magnitude, threatening satellites at altitudes of 8,000 km altitude or so and increasing the radiation dose for satellites undergoing electric orbit raising to GEO.

After many years of experience a set of design guidelines has been established to help protect satellites from internal charging. These include models such as DICTAT (Rodgers et al., 2000), FLUMIC (Wrenn et al., 2000) and MOBE-DIC (Hands et al., 2015, 2020) which have been used for satellite design in Europe for many years, the NASA Technical Handbook (NASA, 2022) and publications by the European Cooperation for Space Standardization on spacecraft engineering (ECSS, 2019). These documents recommend that if the incident flux is greater than 0.1 pA cm^{-2} then there should be additional shielding to reduce the charging current to less than 0.1 pA cm^{-2} for any period of 10 hr, and less than 0.02 pA cm^{-2} if the temperatures less than 25°C. Approximately 2.80 mm (110 mils) of Al shielding (or its equivalent) is recommended for geostationary orbit (GEO). The shielding is quoted in mils, where 1 mil is one thousandth of an inch or 0.0254 mm. These guidelines are based on a current-density approach which is applicable to thick absorbers.

The recommendation on how much shielding to use is based on examples of the worst-case electron environment experienced by several spacecraft, including ATS 5 and 6, SCATHA, and CRRES (e.g., Fennell et al., 2000). While this has served the satellite industry very well, it does not give any indication of how often this type of environment occurs. For example, many satellites continue operations beyond their design life which suggests there could be some over protection which adds to the cost of a spacecraft. On the other hand, it is not clear if the recommended shielding would be sufficient to withstand a storm as big as the 1859 Carrington storm (Tsurutani et al., 2003), multiple storms in quick succession (Meredith et al., 2015) or fast solar wind streams which result in some of the highest electron flux inside the Earth's magnetic field (Horne et al., 2018).

One of the ways of addressing these issues is to use a statistical approach. For example, the electron flux for a 1 in n-year event has been published for GEO using GOES data (Koons, 2001; Meredith et al., 2015; O'Brien et al., 2007), for medium Earth orbit using GIOVE plate currents (Meredith, Horne, Isles, & Green, 2016) and for LEO using POES electron data (Meredith, Horne, Isles, & Green, 2016). More recently the electron flux for a 1 in 10, 1 in 50 and 1 in 100-year event has been published for a range of L shells including GEO using electron data from one of the GPS satellites (NS41) (Meredith et al., 2023). The advantage of these results is that they use methods of extreme value statistics to obtain the electron flux which takes into account that the probability distribution of events is non-Gaussian. The results from NS41 in particular provide the electron spectrum over a range of energies appropriate to internal charging. Furthermore, a 1 in 100-year event has come to be recognized as a reasonable worst-case (e.g., Hapgood et al., 2021) that has been adopted in policy documents to develop a severe space weather preparedness strategy in the UK (UKSSWPS, 2001). Although there may be events where the flux could be even higher for short periods, and in some situations a soft spectrum could be more hazardous than a hard spectrum, we shall adopt values corresponding to a 1 in 100-year event in the work below as a reasonable worst-case, unless otherwise stated.

The purpose of this paper is to evaluate satellite charging at GEO for a reasonable worst-case and compare it to the NASA and ECSS guidelines. We also evaluate charging for satellites in lower equatorial orbit which are important for satellites undergoing electric orbit raising to GEO and Global Navigation Satellite System constellations such as GPS and Galileo which can pass through the equatorial region for an non-negligible amount of time.

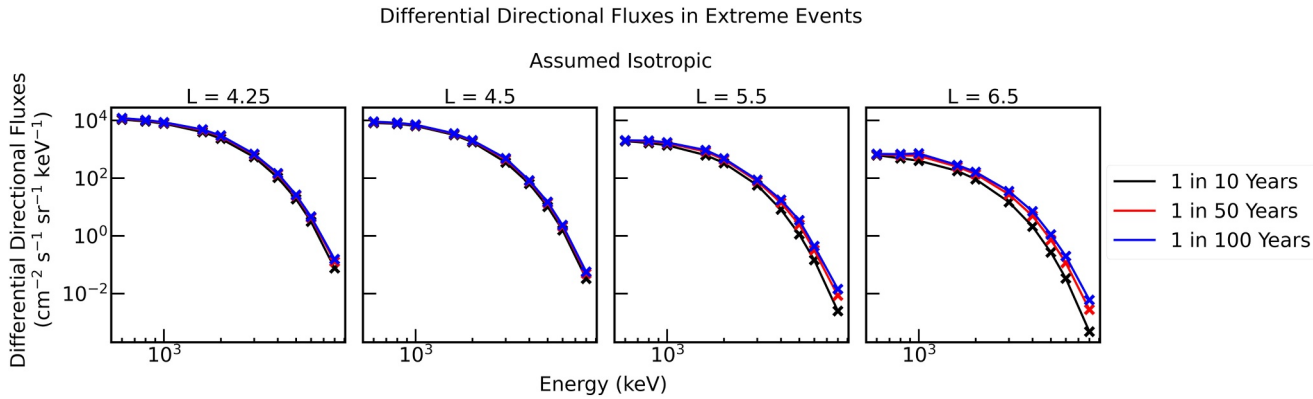

Figure 1. Directional differential electron spectrum for different L shells for (black) a 1 in 10-year, (red) 1 in 50-year, and (blue) 1 in 100-year event. The data are from GPS satellite NS41. Only data at $L = 4.17$ (not shown) were taken at the magnetic equator, the data at larger L correspond to higher latitudes.

2. Reasonable Worst-Case

Figure 1 shows the daily average electron flux for a range of L shells and for a range of 1 in n-year events, adapted from Meredith et al. (2023). Here L is the McIlwain L and will be used in the rest of this paper. These data were recorded by GPS satellite NS41 which was in an inclined circular orbit ($i = 55°$), and crossed the equator at approximately 20,200 km altitude or $L = 4.17$. Thus while the data at $L = 4.17$ are taken at the magnetic equator, the data at larger L were taken at higher latitudes.

It is interesting to note that in Figure 1, there is very little difference between the 1 in 10 and 1 in 100-year flux at $L = 4.25 - 5.0$. There is a larger variation in flux at larger L, for example, near $L = 5$, but even here the variation is within a factor of 2 or so. This suggests that there is a limiting upper value to the flux that is controlled by one or more physical processes. The largest flux at GEO occurs during weak storms driven by fast solar wind streams, or multiple storms, and not large magnetic storms (Horne et al., 2018; Meredith et al., 2015).

Electron distributions observed at the equator are often observed to have some pitch angle anisotropy, peaked perpendicular to the magnetic field, but this would not be observed by the GPS satellites on larger L shells. For example, GPS satellites cross $L = 6.5$ over a range of latitudes between 30° to 40° (Morley et al., 2016; Figure 3). At these latitudes mirroring electrons have an equatorial pitch angle of 34° to 21°, respectively, and so NS41 would only detect that part of the equatorial distribution less than these angles. Analysis of the CRRES data (Horne et al., 2003) shows that the pitch angle distribution can become peaked for short periods as a result of acceleration by chorus plasma waves. Observations from Van Allen Probes also show that the distribution at $L = 4.25$ can be anisotropic and vary by a factor of five or so between 30° and 90° for particular events (Olifer et al., 2022). Previous work has also shown (Shi et al., 2016) that if the pitch angle distribution is represented as $\sin^n \alpha$ then for energies greater than 600 keV and $L > 4$ n lies in the range $0 \le n \le 2$ for high geomagnetic activity ($Kp > 4$).

To take this anisotropy into account we used a normalized equatorial pitch angle distribution with $J(\alpha) = \sin^n \alpha$ and $n = 2$ corresponding to high geomagnetic activity which is appropriate for a 1 in n-year event. The distribution was mapped to higher latitudes using Liouville's theorem and the omnidirectional flux was computed by integrating over pitch angles. The omnidirectional flux was then compared to data from NS41 and scaled. The scaling was then applied to the equatorial distribution.

Figure 2 shows the resulting electron flux that has been mapped to the magnetic equator and adapted for the anisotropy (in red). Data from the AE9 model (version 1.58.001) using a perturbed mean with the 99 percentile is also shown for comparison, together with the maximum daily averaged equatorial flux at 270 keV, 625 keV and 2.65 MeV observed by the LANL satellites at GEO, shown as light blue data points (O'Brien et al., 2007) for $L = 6.5$, with the 95% confidence limits. Although the LANL and GPS data are included in the AE9 model (Ginet et al., 2013), the data point at 2.65 MeV lies between the GPS data and the AE9 model while the data at lower energies lies close to the AE9 model, indicating good agreement.

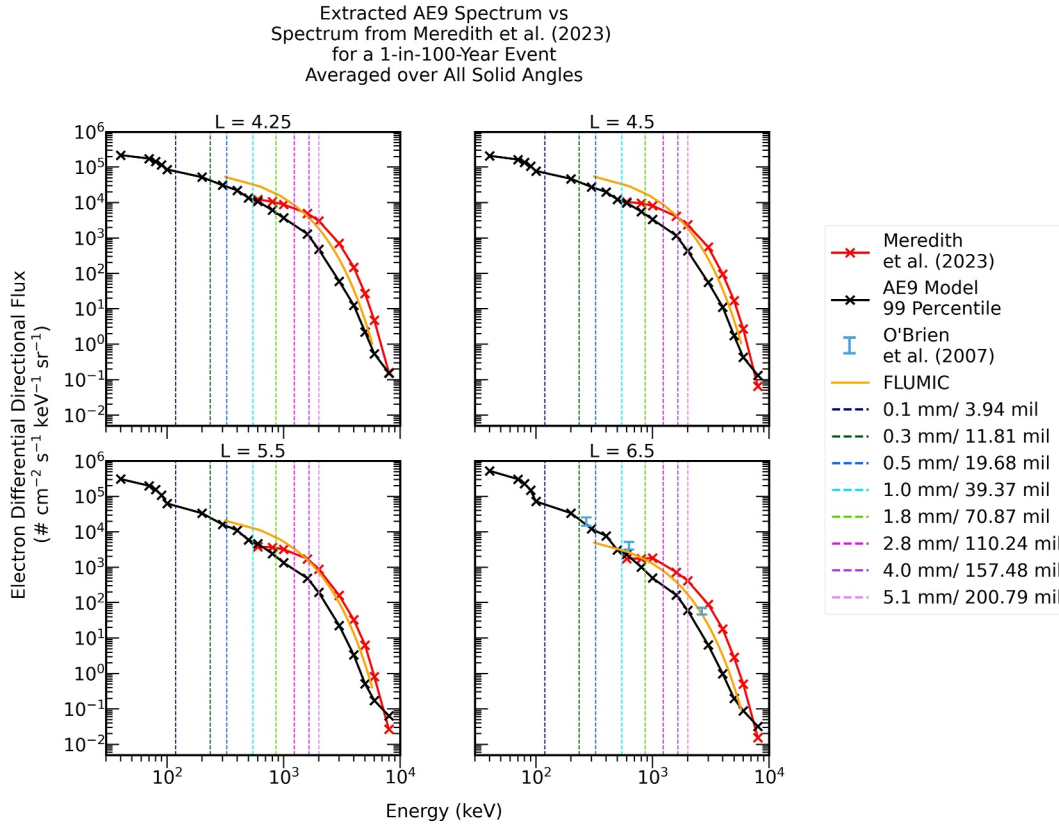

Figure 2. Daily average differential directional electron flux as a function of energy for different L at the magnetic equator. The data for a 1 in-100 year event are shown in red and for the 99 percentile from the AE9 model are in black. The vertical dashed lines show the approximate energy for different levels of shielding above which electrons would begin to penetrate the shielding.

Figure 2 also includes differential electron flux calculated using the FLUMIC model, version 3.0 (Wrenn et al., 2000), available via the SPENVIS web site (see data statement). The FLUMIC model is based on an exponential spectrum and was calculated for the declining phase of the solar cycle where the flux is highest (fraction of the solar cycle equal to 0.8), and spring equinox (fraction of year equal to 0.216). At energies of a few hundred keV the flux is slightly higher than the AE9 model, but at higher energies, typically greater than 2 MeV, it lies between AE9 and the data from Meredith et al. (2023) adjusted and mapped to the equator as described above.

To calculate the charging current penetrating different levels of shielding we used version 4.2 of the DICTAT code which uses a current-density limit approach (Rodgers et al., 2000). The code is available from the European Space Agency web site (see data statement below). We used planar geometry with flux incident on one side. Since DICTAT requires an integral directional incident flux, and that the flux be isotropic, we integrated the directional differential flux over solid angle, which includes the anisotropy, and energy to get the omnidirectional integral flux and then divided by 4π. This was used as the incident flux.

To calculate the charging current for low levels of shielding the energy spectra in Figure 2 was extended from 600 keV down to 40 keV using the AE9 model to calculate the differential flux as a function of energy for the 99 percentile. To obtain the reasonable worst-case we used the electron flux from either the 1 in 100-year event, or the 99 percentile, whichever was higher at each energy. For example, at $L = 6.5$, for $E < 600$ keV the flux is taken from AE9 and at higher energies it is taken from the 1 in 100-year flux, except for the highest energy data point. We chose to use these two data sets as they are based on a statistical analysis of data rather than the FLUMIC model which is based on an exponential fit.

In this study, the term "charging current" refers to the maximum equilibrium current flowing at any location inside the dielectric. At GEO ($L = 6.6$) Figure 3 shows that 2.8 mm of Al (magenta line) shielding is just

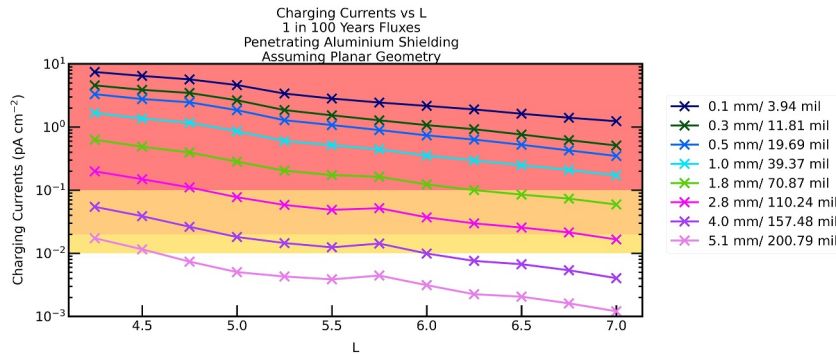

Figure 3. Charging current per unit surface area penetrating different levels of Al shielding as a function of L for equatorial orbit using daily averaged flux. Geostationary orbit is at $L = 6.6$. GPS satellites cross the equator at $L = 4.17$ and Galileo at $L = 4.65$.

sufficient to keep the charging current around 0.02 pA cm^{-2}, and well below the recommended guideline of 0.1 pA cm^{-2} (shown by the red shading) during a reasonable worst-case. In fact 1.8 mm of Al would keep the charging current below recommended guideline but without any margin of error. The calculation here is for the daily average electron flux, so the charging current could be larger than this, but only for short periods of a few hours.

At lower L more shielding would be required. For example, using the recommendation of 2.8 mm of Al shielding at GEO, approximately 4.5 mm (177 mil) of Al shielding would be required to offer the same level of protection for a satellite in equatorial orbit at $L = 4.5$.

More generally, Figure 3 can be used as a guide for amount of shielding required to survive a reasonable worst-case for satellites in circular equatorial orbits between 4.25 and 7.0 Re (20,702 and 38,220 km altitude). We note that it is possible to calculate charging currents using DICTAT and FLUMIC models (Wrenn et al., 2000) via the SPENVIS web site (see data statement), where FLUMIC gives a slightly lower flux at higher energies, for example, see Figure 2.

GNSS satellites such as the GPS and Galileo constellations are in inclined orbits (55° and 56°, respectively) and cross the equator at (GPS) $L = 4.17$ and (Galileo) $L = 4.65$ twice per orbit. Thus the charging current varies considerably along the orbit and would only peak near the equatorial crossing.

We conclude that shielded components are protected against internal charging at GEO using the existing guidelines. However, components such as cables and connectors are often located just underneath the surface of the spacecraft but they are not shielded to the same level as this would require significant additional mass. Consequently these cables can be vulnerable to dielectric breakdown. We consider this next.

3. Electric Field in a Dielectric

Honeycomb sandwich structures made out of Al are widely used in the construction of satellites due to their lightweight properties combined with high strength and good thermal insulation (e.g., Figure 1 of Boudjemai et al. (2012)). A typical design is a structure consisting of two thin Al sheets, one at the top and one at the bottom, with a hexagonal grid between them. The thickness of the Al sheets may vary but typical values are between 0.3 and 1 mm of Al depending on the design choice. The hexagonal grid may have a side length of 5 mm and a wall thickness of 0.03 mm. For comparison standard household Al foil has a thickness of 0.016 mm. The separation between the two face sheets may vary from 20 to 30 cm. Note that in this design it is possible for electrons to penetrate the upper and lower face sheets into the spacecraft without going through the side walls of the honeycomb. Thus the protection offered by the outer honeycomb structure could vary between a few tenths to a few mm of Al.

Coaxial cables can be more susceptible to discharges than other components due to the exceptionally high resistivity in the dielectric layer of the cable. As electrons penetrate the outer shield, some will become absorbed in

the dielectric and an electric field will build up. If the field exceeds the breakdown field of the material (also known as the dielectric strength) then an electrostatic discharge is likely to occur and may cause an anomaly.

To calculate the maximum electric field, $E_{\max}$, and the change in conductivity of a typical insulator around a co-axial cable we used the DICTAT code (Rodgers et al., 2000). In DICTAT the electric field at any layer of the dielectric is given by

$$E(t_n) = \frac{J_{in}(t_n)}{\sigma(t_n)}\left(1 - \exp\left(-\frac{\Delta t}{\tau(t_n)}\right)\right) + E(t_{n-1})\left(\exp\left(-\frac{\Delta t}{\tau(t_n)}\right)\right) \quad (1)$$

The full derivation is included in the Appendix A. Because radiation of different energies have different penetration depths, the dielectric is modeled as a series of ten sub-layers where each layer is treated as a leaky capacitor. The first term represents an increase in the electric field due to direct charge deposition, and due to currents leaving an adjacent layer. The second term represents the decay due to leakage currents. Thus, the electric field is time varying. The current J_{in} is calculated from the incident flux of particles and currents from adjacent layers and the time constant $\tau = \epsilon/\sigma$ is determined by the properties of the insulating material. The conductivity σ is not constant but is given by

$$\sigma = \sigma(E,T) + \sigma_r \quad (2)$$

The conductivity varies with high electric fields (above about 10^6V m^{-1}) according to Adamec and Calderwood (1975)

$$\sigma(E,T) = \sigma(T)\left(\frac{1}{3}\left(2 + \cosh\left(\frac{\beta_F E^{0.5}}{2k_B T}\right)\right)\right)\left(\frac{2k_B T}{eE\delta}\sinh\left(\frac{eE\delta}{2k_B T}\right)\right) \quad (3)$$

where $\beta_F = \sqrt{e^3/(\pi\epsilon)}$, δ is an experimentally derived parameter equal to 10^{-9} m, k_B is Boltzmann's constant and e is the electronic charge. Here the dielectric permittivity is given by $\epsilon = \epsilon_0\epsilon_r$ where ϵ_r is the relative permittivity. The temperature dependence is given by

$$\sigma(T) = \sigma_0 \exp\left(-\frac{E_A}{k_B T}\right) \quad (4)$$

where E_A is an activation energy. The radiation induced conductivity (RIC) σ_r is given by Fowler (1956), Frederickson (1977), Hastings and Garrett (2004)

$$\sigma_r = k_p \dot{D}^{\Delta} \quad (5)$$

where $\dot{D}^{\Delta}$ is the dose rate and the parameters k_p and Δ have been determined empirically. In these calculations the incident electron flux remains constant but the time constant τ varies in time with the changes in conductivity across different dielectric sub-layers (e.g., Paulmier et al., 2015; Gillespie, 2013; Frederickson, 1977).

The DICTAT code can only simulate three layers of different materials, a grounded shielding layer, a dielectric and an underlying conductor which can be grounded (or not). We used this simple geometry where the shielding layer represents the outer surface of the spacecraft and shielding on the cable, the dielectric represents the outer insulating layer of a co-axial cable and the third layer is the internal conductor. We calculated the evolution of $E_{\max}$ in the dielectric and the change in conductivity as a function of time. We selected Teflon (Polytetrafluoroethylene, PTFE) to represent the dielectric material with a thickness of 0.1 cm and $\epsilon_r = 2.15$, (obtained from the NASA handbook, NASA, 2022) because it is used in coaxial cables, and its properties are similar to its common alternatives. The conductivity due to thermally excited electrons is negligible for insulators (Gillespie, 2013) and therefore we set $E_A = 0$. We also set $\sigma_0 = 10^{-16}$ Ohm^{-1} m^{-1}, which is the approximate conductivity at room temperature (25°C) (NASA, 2022). RIC does have a temperature dependence (e.g., see Gillespie, 2013 for a detailed analysis) but we initially set this term to zero by setting $k_p = 0$ and varied this later (Section 5). As before, $E_{\max}$ was calculated with planar geometry.

10.1029/2024SW004226

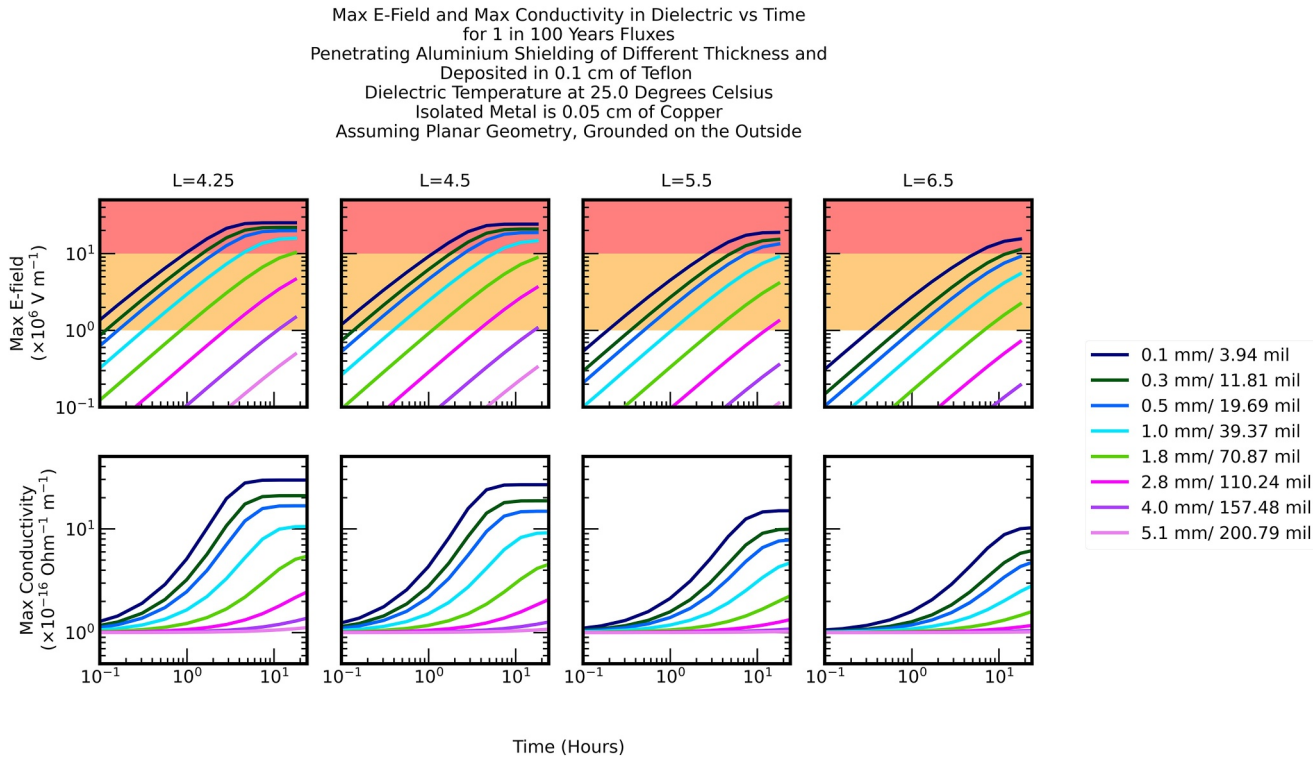

Figure 4. Time evolution of the (top row) maximum electric field and (bottom row) the maximum conductivity in Teflon for a 1 in 100-year event for different levels of Al shielding. The orange and red shading indicate the approximate breakdown electric field of the material.

The breakdown electric field for dielectrics such as Teflon can vary by orders of magnitude due to its sensitivity to extrinsic factors, such as manufacturing limitations, blemishes, handling damage, etc. It is very difficult to produce a theoretical model to predict the dielectric strength due to its intrinsic structural disorder. However, laboratory experiments using an electron beam and scattering plates to form a space-like electron spectrum called GEODUR have been done for different levels of shielding. In these experiments the breakdown field varied between 10^6 and 10^7 V m^{-1} (e.g., Figure 12 of Rodgers et al. (2000)). Moreover, Andersen et al. (2017) calculated that the extreme lower bound of dielectric strength is on the order of 10^6 V m^{-1}.

The results of these studies suggest that electric fields between 10^6 and 10^7 V m^{-1} may have a non-negligible chance of discharge and are shown in orange in Figure 4. Values $>10^7$ V m^{-1} are shown in red.

Figure 4 (top row) shows how the maximum electric field in the dielectric increases with time for different L. At $L = 4.25$ the maximum electric field inside the material E_{max} rises rapidly and exceeds 10^7 V m^{-1} after approximately 2 hr for 0.5 mm (blue curve), and 20 hr for 1.8 mm (green). This is due to the higher flux at lower L, as shown in Figure 2.

In comparison, at $L = 6.5$ E_{max} does not increase quite so quickly. For 0.1 mm of shielding (dark blue curve), E_{max} exceeds 10^7 V m^{-1} after 15 hr. In general the rate of increase slows down after about 12 hr, although E_{max} is still increasing after 24 hr and E_{max} tends to level off as charge deposition becomes comparable to charge leakage. In general, it takes longer for E_{max} to reach a maximum if the shielding is increased, as might be expected since more shielding means fewer penetrating electrons. Thus the amount of shielding provided by the outer surface of the spacecraft is a key factor.

The conductivity (bottom row) increases significantly as E_{max} increases above about 10^6 V m^{-1}. This is an effect of high electric fields in a dielectric (Adamec & Calderwood, 1975). Note that the conductivity increases by over an order of magnitude for lower levels of shielding compared to the higher levels. We also note that if the conductivity of Teflon is lower, as some recent measurements suggest (Gillespie, 2013), then from Equation 1 the electric field would be larger and would reach the breakdown field even faster.

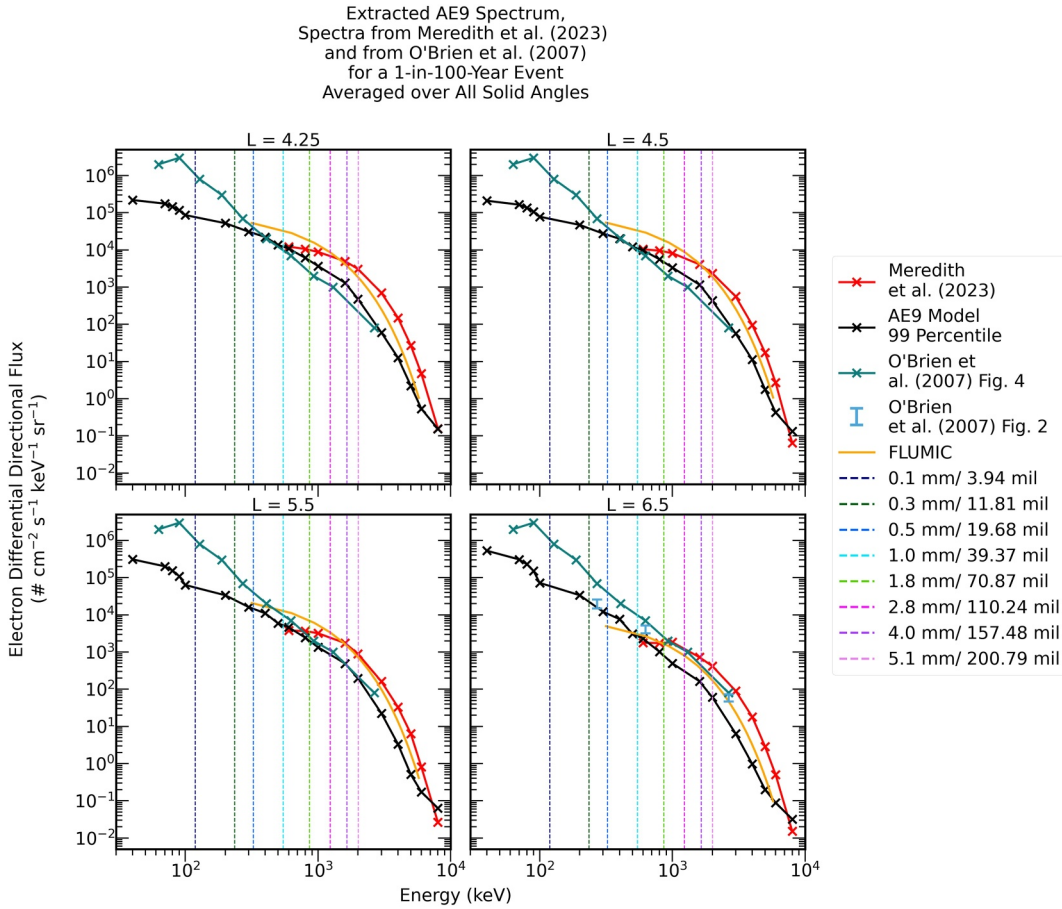

Figure 5. Electron flux as in Figure 2, but (in dark green) with the data from (O'Brien et al., 2007) at lower energies averaged over 1 hr instead of 24 hr. The flux at low energy is the same in each panel.

4. Low Energy Electron Flux >50 keV

Lower levels of shielding enable lower energy electrons to penetrate the spacecraft, as illustrated by the vertical dashed lines in Figure 2. For example, reducing the shielding to 0.1 mm would let electrons of 100 keV and above to penetrate the shield. At these energies the electron flux can be highly variable for short periods, for example, during substorms. As Figure 4 shows that E_{max} can increase on a timescale of a few hours for this level of shielding, it is appropriate to consider flux levels that occur during substorms and other related events which affect this energy range.

The maximum differential electron flux at energies of tens to hundreds of keV has been calculated in different ways by previous authors. The maximum stably trapped flux was calculated by Kennel and Petschek (1966) by assuming that as the flux increased during substorms the anisotropy of the distribution would excite strong whistler mode waves which would then diffuse electrons into the loss cone causing losses, and hence effectively regulate the trapped flux. By balancing wave growth, particle diffusion and the propagation of energy out of the unstable region they were able to calculate the trapped flux (Kennel & Petschek, 1966). This work was done before it was realized that chorus waves can accelerate part of the trapped flux to relativistic energies (e.g., Horne, Thorne, Glauert, et al., 2005). More recently the trapped flux has been calculated for higher energies (Mauk & Fox, 2010; Olifer et al., 2021, 2022). An alternate way has been to use extreme value statistics to analyze the data from the LANL satellites at GEO (O'Brien et al., 2007). Since this method was based on observed data, and takes into account non-Gaussian distributions of events, we have used data from (O'Brien et al., 2007) for our analysis here.

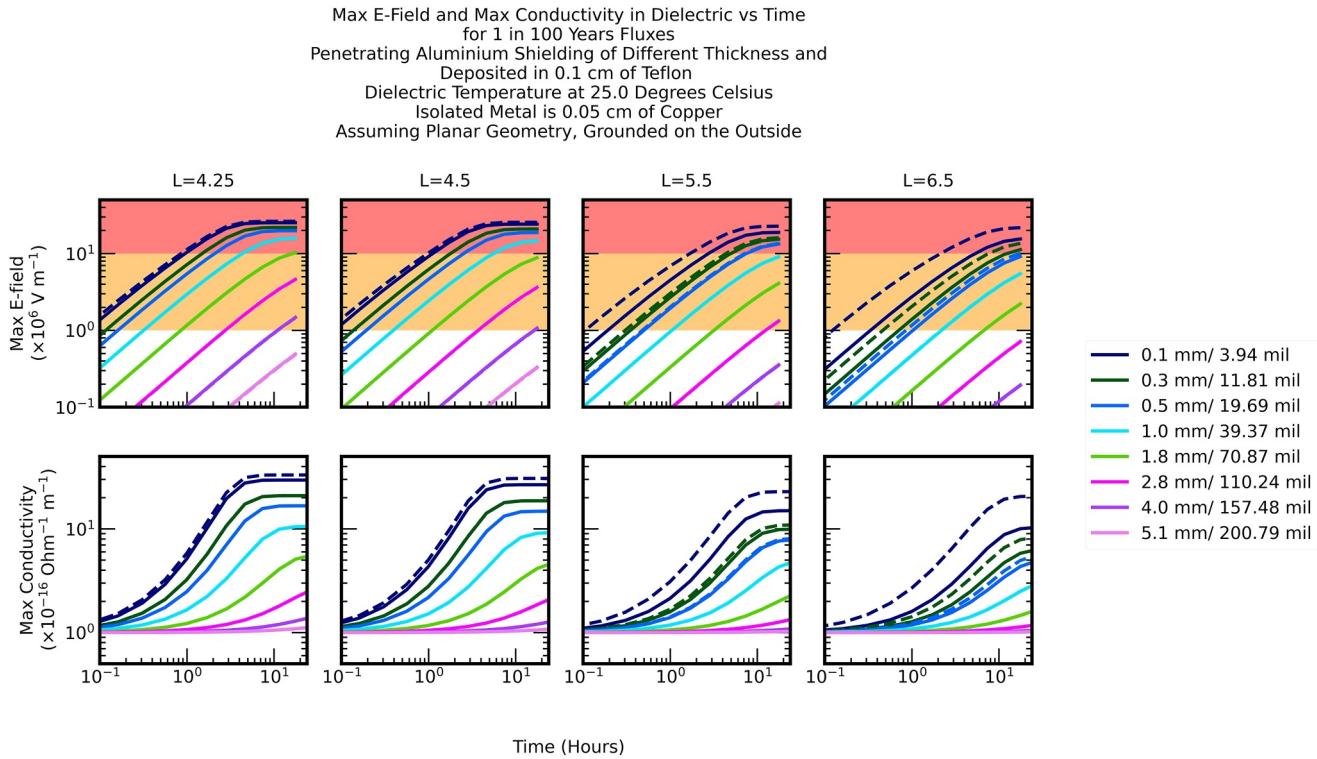

Figure 6. Maximum electric field for the reasonable worst-case with (dashed) the higher 1 hr low energy electron flux and (solid) without. Shown are the (top row) maximum electric field and (bottom row) the maximum conductivity in Teflon. The yellow and red shading indicates the approximate break-down electric field of the material (Teflon). Note that the lower energy flux may decrease after 1 hr.

Figure 5 shows the electron flux from Figure 2, as before, but with LANL satellite data at lower energies (shown in dark green) from (O'Brien et al., 2007). The data were for the worst-case averaged over 1 hr instead of 24 to capture the variability at low energies caused by substorm injections. Note that the flux at different energies were not measured at the same time, they are the maximum values that occurred at different times. We have put them together here as a reasonable worst-case. The data extend down to 64 keV. Although the LANL data were taken at GEO, electron injections can penetrate to much lower L and overlap the plasmapause during storms and substorms. We have therefore assumed that the same low energy spectrum for all $L \geq 4.25$. For comparison the maximum trapped flux calculated by Olifer et al. (2021) using the theory of Kennel and Petschek at $L = 4.25$ and 168 keV was approximately 2×10^5 cm^{-2} s^{-1} sr^{-1} keV^{-1} which is just a little lower, but comparable to the measured spectrum shown here. The peak around 90 keV of the hourly averaged data could be the result of bremsstrahlung contamination (O'Brien et al., 2007) but this only affects results with the lowest levels of shielding of around 0.1 mm of Al. The flux in Figure 5 now forms our reasonable worst-case for all energies.

Figure 6 shows that at $L = 4.25$ there is very little difference between E_{max} (dashed lines) and the earlier result (solid lines) when the flux at the lower part of the energy spectrum is increased. E_{max} is slightly higher than before for 0.1 mm of Al shielding. The biggest differences are at larger L, for example, $L = 6.5$. In this case E_{max} reaches higher values more quickly than before as the conductivity increases more quickly (Figure 6, bottom right).

The results suggest that the maximum electric field inside a dielectric such as Teflon could exceed the breakdown field as a result of electron injections at energies of tens to hundreds of keV if the flux remains elevated for more than an hour or so. This result agrees well with previous work where substorms have been associated with satellite charging and anomalies on the nightside and around toward dawn (Fennell et al., 2000). Electrons injected by substorms drift under the influence of the enhanced convection electric field from the nightside through dawn and may take hours to decay. The results here suggest that it is these electrons that become buried in the dielectrics of cables underneath the surface of the spacecraft that are likely to pose the highest risk of an anomaly. This could be mitigated by including more grounded shielding around the coaxial cables or thicker face sheets.

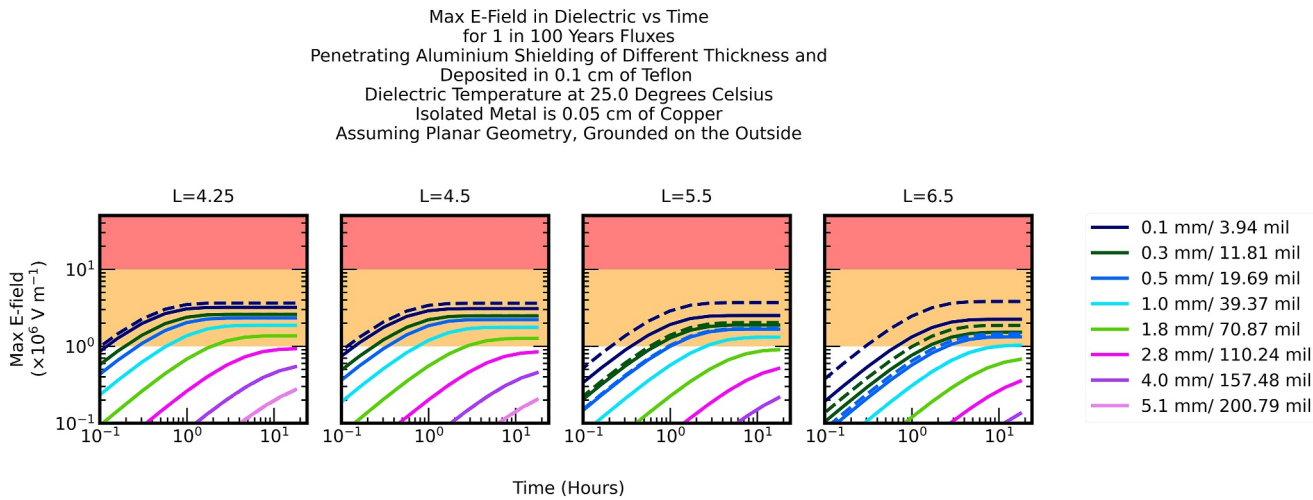

Figure 7. Maximum electric field with radiation induced conductivity for the reasonable worst-case with (dashed) the higher 1 hr low energy electron flux and (solid) without. The yellow and red shading indicates the approximate break-down electric field of the material (Teflon). Note that the lower energy flux may decrease after 1 hr.

5. Effects of Radiation Induced Conductivity (RIC)

Ionizing radiation changes the structure of dielectrics, which induces changes to the conductivity (e.g., Fowler, 1956; Frederickson, 1977; Gillespie, 2013; Gross et al., 1980; Khatipov, 2001; Paulmier et al., 2015). This RIC is very difficult to measure but there are some data available where samples have been irradiated in a chamber by electron beams for periods from a few minutes to several hours (e.g., Gillespie, 2013; Paulmier et al., 2015). By fitting the data the parameters k_p and Δ have been determined for FEP Teflon and agree to within a factor of two or so with direct measurements (Rodgers et al., 2003).

To test the importance of RIC we first set $k_p = 2.0 \times 10^{-14}$ and $\Delta = 0.7$, as given in the documentation available with DICTAT, and similar to the data reported by Rodgers et al. (2003). The dose rate due to electrons is included in the code but not that due to ions, cosmic rays or gamma rays. However, since our focus is outside the proton radiation belt and the cosmic ray flux is much lower than the radiation belt electron flux this should be a reasonable approximation.

Figure 7 shows the effects of including RIC using the same flux spectra as before. E_{max} is significantly reduced for lower levels of shielding but still exceeds 10^6 V m^{-1}, the estimated lower limit of the breakdown field (Andersen et al., 2017). In general the risk of an anomaly is reduced, but not removed.

To test the sensitivity of the results to RIC Figure 8 shows the same calculations but with $k_p = 10^{-13}$ and $\Delta = 1.0$ (NASA, 2022). In this case the electric field stays below 10^6 V m^{-1} and is unlikely to reach the breakdown threshold.

6. Discussion

There are several experimental observations of the breakdown field of materials such as Teflon but it is still very difficult to give a precise assessment of whether an anomaly would occur or not as there are so many variables. For example, we have taken values greater than 10^6 V m^{-1} as a guide based on laboratory experiments (Andersen et al., 2017), but there is some uncertainty in this value, it could be higher. We have also used the conductivity of Teflon at room temperature, but the temperature of satellite components in space can drop to near freezing, especially during eclipse periods. If this results in even lower electrical conductivity this could mean it takes longer to reach the breakdown field. Furthermore, as discussed above, estimates of the parameters used for RIC vary by four orders of magnitude (NASA, 2022). We have used relatively high values based on experimental measurements, which tend to reduce the risk of an ESD, but if the true values are smaller then the risk is higher. In general we require more experimental measurements to reduce these uncertainties.

10.1029/2024SW004226

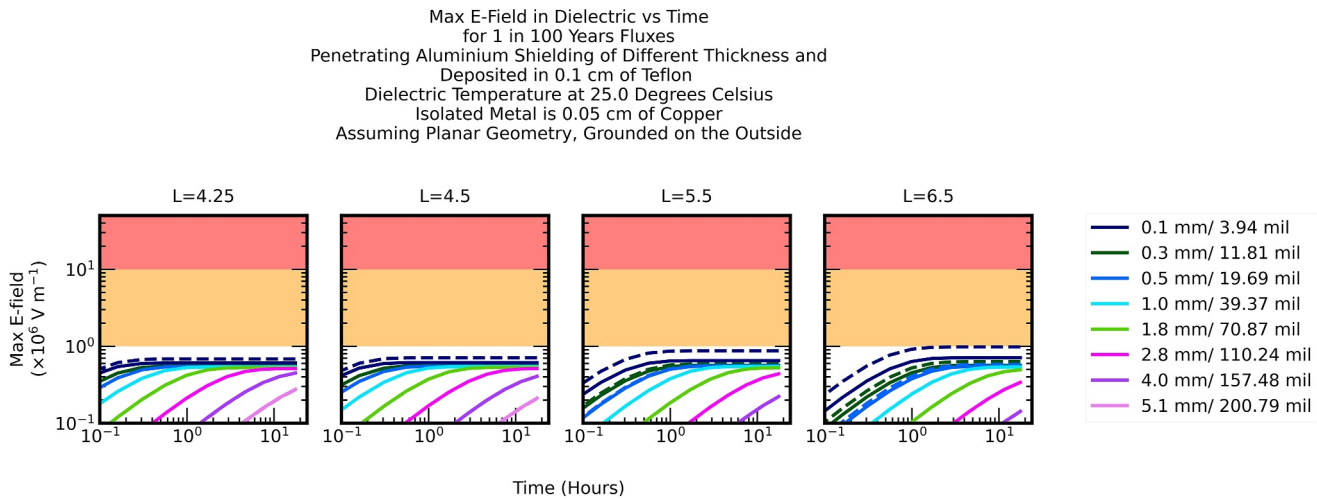

Figure 8. Same calculations as Figure 7, but with higher radiation induced conductivity. Note that the lower energy flux may decrease after 1 hr.

Satellites such as the GPS and Galileo constellations are in an inclined circular orbit and cross the equator at approximately $L = 4.17$ and 4.65. The actual level of shielding used in these satellites is not publicly available. Using satellite two line elements and the Olsen Pfitzer quiet magnetic field model (Olson & Pfitzer, 1977) we estimate that a GPS satellite could remain in a high flux region for 60–90 min as it crosses the equator. Figure 7 shows that for a 1 in 100-year event, the internal electric field inside a coaxial cable just under the surface of a spacecraft could come close to or exceed the breakdown field on this timescale if there are low levels of shielding offered by the surface of the spacecraft.

One of the questions that has never been answered satisfactorily is why only one satellite at GEO should suffer an anomaly leading to service outage if it is one of a fleet of satellites all designed to the same specification (Bodeau, 2010). One might expect all the satellites to be affected. One possible reason is that the radiation dose varies with longitude around the geostationary arc due to the non-uniformity of the Earth's magnetic field. For example, the $E > 2$ MeV electron flux at GOES West is a factor of 2.5 times higher than that at GOES East since GOES West is at a lower magnetic latitude and hence lower L shell (Meredith et al., 2015). In general satellites located near 20° E and 160° W experience a higher flux than other longitudes. However, one might expect the higher flux to be highly localized to account for an anomaly on just one satellite but this is not the case since the magnetic field varies smoothly around the geostationary arc. There may of course be slight differences in the actual construction, or materials used in the construction, and many other factors. Aside from this we suggest the following scenario. During an event that increases the electron flux many spacecraft will become charged and an electric field will build up in the dielectrics. The electric field may not reach the breakdown threshold, but the charge may take hours or days to leak away and decay (Bodeau, 2010). Thus many satellites would be charged and at higher risk. The deciding factor may be a cosmic ray or energetic heavy ion which passes through a sensitive region of the dielectric or electronic component creating a trail of ionization which triggers a discharge leading to an anomaly. Since the flux of cosmic rays is so low, this would explain why only one out of a fleet of satellites would be affected. A magnetic storm, series of storms, or high speed solar wind stream that increases the trapped electron flux accompanied by a large solar energetic particle event might present a much higher risk of anomalies on several satellites. It would be interesting to test this idea experimentally.

It is important to note that once a satellite has suffered a non-fatal anomaly, it may then have a higher sensitivity to the radiation environment such that the same or similar anomalies may occur again for lower levels of electron flux. This seems to have happened with a spacecraft at GEO referred to as DRAδ (Wrenn, 1995) which suffered over 200 anomalies over a 10 year period (Wrenn et al., 2002). Forecasts of the electron flux in the radiation belts can then help operators plan their operations and warn users when service might become unreliable. Operators would need to calibrate the flux level according to their particular needs.

Electric orbit raising to GEO is becoming increasingly common. It takes typically 200 days to reach final orbit, and several days may be spent in regions of high flux near the equator. If a space weather event took place, leading to a reasonable worst-case electron flux as described above, this could significantly increase the risk of damage en route to GEO. For very valuable payloads, the protection for this type of scenario ought to be considered.

7. Conclusions

We have conducted an analysis of satellite charging for a reasonable worst-case space weather event, which is taken here as a 1 in 100-year event for a range of circular equatorial orbits between 4.25 and 6.5 Re. The differential electron flux between 600 keV and 8 MeV were taken from an extreme value analysis of data from the GPS satellite NS41 and extended down to lower energies (40 keV) using the 99 percentile of the AE9 model. The spectrum below 600 keV was later modified to use the flux corresponding to the 1 hr averaged worst-case measured by the LANL satellites at GEO. We used the DICTAT code to calculate the charging current behind different levels of shielding and the maximum electric field inside the dielectric of a coaxial cable. The main conclusions of our study are:

1. The recommended level of shielding (typically at least 2.8 mm of Al or 110 mils) provided by the NASA and ECSS guidelines is sufficient to prevent serious internal charging at geostationary (geosynchronous) orbit for a reasonable worst-case.
2. Our results can be used to assess the level of shielding required for circular equatorial orbits between $4.25 \leq L \leq 7$ (20,700 and 38,220 km altitude). For example, using the recommendation of 2.8 mm of Al shielding at GEO, approximately 4.5 mm (177 mils) of Al shielding would be required to offer the same level of protection for a satellite in equatorial orbit at $L = 4.5$.
3. Our reasonable worst-case shows that the maximum electric field could exceed the breakdown field for dielectrics in coaxial cables just underneath the honeycomb surface of a spacecraft on a timescale of 1–2 hr. This could result in ESD and an anomaly.
4. RIC reduces the risk of reaching the breakdown field, but is highly uncertain. More experimental measurements on RIC are needed to reduce the uncertainty.
5. Satellites at GEO on the night side of the Earth and early morning local time are most at risk due to the prevalence of electron injections at tens to hundreds of keV during substorms in this region.
6. A reasonable worst-case event could significantly increase the risk of damage for satellites undergoing electric orbit raising to GEO.

We suggest that even if the charging current is not sufficient for the electric field to reach the breakdown field, satellites may remain in a charged state for hours, possibly days, and are therefore more at risk from a cosmic ray or high energy ion which passes through a sensitive region of the dielectric or electronic component creating a trail of ionization which triggers a discharge leading to an anomaly. A magnetic storm, series of storms, or fast solar wind streams that increases the electron flux and accompanied by a large solar energetic particle event would present a much higher risk of anomalies on several satellites. It would be interesting to test this suggestion experimentally.

Appendix A: Electric Field Within a Dielectric

For a parallel plate capacitor, the electric field can be calculated with Gauss' law to be:

$$E(t) = \frac{Q(t)}{A\epsilon} \tag{A1}$$

where $Q(t)$ is the charge accumulated on the plate at a certain time t, ϵ is the dielectric permittivity, and A is the area of the plate. At every moment, the plate would receive more charges because of the current going into the plate $J_{in} = I_{in}/A$. However, because the dielectric is not a perfect insulator, it leaks charges to the opposite plate because of the electric field that it itself has accumulated. This current leaving the plate J_{out} can be found by Ohm's law:

$$J_{out}(t) = \sigma(t)E(t) \tag{A2}$$

where σ is the conductivity of the dielectric. Therefore, the rate of change of the charges of the plate is given by

$$\begin{aligned}\frac{dQ(t)}{dt} &= A[J_{in}(t) - J_{out}(t)] \\ &= A[J_{in}(t) - \sigma(t)E(t)]\end{aligned} \tag{A3}$$

Taking the time derivative of the electric field,

$$\begin{aligned}\frac{dE(t)}{dt} &= \frac{1}{\epsilon}\left[\frac{1}{A}\frac{dQ(t)}{dt}\right] \\ &= \frac{J_{in}(t)}{\epsilon} - \frac{\sigma(t)}{\epsilon}E(t) \\ &= \frac{J_{in}(t)}{\epsilon} - \frac{E(t)}{\tau(t)}\end{aligned} \tag{A4}$$

It can then be easily shown that, in the limit that $\Delta t \to 0$, the equation that DICTAT proposes

$$E(t_n) = \frac{J_{in}(t_n)}{\sigma(t_n)}\left(1 - \exp\left(-\frac{\Delta t}{\tau(t_n)}\right)\right) + E(t_{n-1})\left(\exp\left(-\frac{\Delta t}{\tau(t_n)}\right)\right) \tag{A5}$$

is equivalent to the equation above for $\frac{dE(t)}{dt}$, making it a valid solution. Here, $\tau(t) = \epsilon/\sigma(t)$.

Because the conductivity changes at different depths of the dielectric, DICTAT models the dielectric as a series of capacitors when calculating the electric fields.

Data Availability Statement

The files containing data used to create the figures in the paper are available via (Lam et al., 2024). The documentation and code for DICTAT version 4.2 are available from https://essr.esa.int/project/dictat. The SaRIF web site can be accessed via the ESA space weather portal https://swe.ssa.esa.int. The SPENVIS web site can be accessed via www.spenvis.oma.be.

Acknowledgments
We thank D. Rodgers, D. Wade, D. Pitchford, A. Monham and D. Heynderickx for many helpful discussions. RBH, PYL, SAGL, NPM, and PK were supported in part by Natural Environment Research Council (NERC) Grants NE/V00249X/1 (Sat-Risk), NE/X000389/1, NE/R016038/1, and NE/Y006178/1 (PRESCIENT). We thank the referees for their helpful comments.

References

Adamec, V., & Calderwood, J. H. (1975). Electrical conduction in dielectrics and high fields. *Journal of Physics D*, *8*(5), 551–560. https://doi.org/10.1088/0022-3727/8/5/015

Andersen, A., Dennison, J. R., & Moser, K. (2017). Perspectives on the distributions of ESD breakdowns for spacecraft charging applications. *IEEE Transactions on Plasma Science*, *45*(8), 2031–2035. https://doi.org/10.1109/TPS.2017.2655885

Anderson, P. C. (2012). Characteristics of spacecraft charging in low Earth orbit. *Journal of Geophysical Research*, *117*(A7), A07308. https://doi.org/10.1029/2011JA016875

Baker, D. N., Allen, J. H., Kanekal, S. G., & Reeves, G. D. (1998). Disturbed space environment may have been related to pager satellite failure. *EOS*, *79*(40), 477–492. https://doi.org/10.1029/98EO00359

Baker, D. N., Kanekal, S. G., Li, X., Monk, S. P., Goldstein, J., & Burch, J. L. (2004). An extreme distortion of the Van Allen belt arising from the 'Hallowe'en' solar storm in 2003. *Nature*, *432*(7019), 878–881. https://doi.org/10.1038/nature03116

Bodeau, M. (2010). High energy electron climatology that supports deep charging risk assessment in GEO. In *48th AIAA Aerospace Sciences meeting, 4–7 January 2010, Orlando, Florida, 1–13*. https://doi.org/10.2514/6.2010-1608

Boudjemai, A., Amri, R., Mankour, A., Salem, H., Bouanane, M. H., & Boutchicha, D. (2012). Modal analysis and testing of hexagonal honeycomb plates used for satellite structural design. *Materials and Design*, *35*, 266–275. https://doi.org/10.1016/j.matdes.2011.09.012

Choi, H., Lee, J., Cho, K., Kwak, Y., Cho, I., Park, Y., et al. (2011). Analysis of GEO spacecraft anomalies: Space weather relationships. *Space Weather*, *9*(6), S06001. https://doi.org/10.1029/2010SW000597

ECSS. (2019). European cooperation for space standardisation, ECSS-E-HB-20-06A. In *Space Engineering: Assessment of space worst case charging handbook*. ESTEC.

Fennell, J. F., Koons, H. C., Chen, M. W., & Blake, J. B. (2000). Internal charging: A preliminary environmental specification for satellites. *IEEE Transactions on Plasma Science*, *28*(6), 2029–2036. https://doi.org/10.1109/27.902230

Fennell, J. F., Koons, H. C., Roeder, J. L., & Blake, J. B. (2001). Substorms and magnetic storms from the satellite charging perspective. In *Aerospace Report no TR-2000(8570)-2*. Retrieved from https://apps.dtic.mil/sti/pdfs/ADA388410.pdf

Fowler, J. F. (1956). X-ray induced conductivity in insulating materials. *Proceedings of the Royal Society A*, *236*, 1207. https://doi.org/10.1098/rspa.1956.0149

Frederickson, A. R. (1977). Radiation induced currents and conductivity in dielectrics. *IEEE Transactions on Nuclear Science*, *24*(6), 2532–2539. https://doi.org/10.1109/TNS.1977.4329251

Gillespie, J. (2013). *Measurements of the temperature dependence of radiation induced conductivity in polymeric dielectrics. All Graduate Theses and Dissertations*. Utah State University. Retrieved from https://digitalcommons.usu.edu/etd/1953

Ginet, G. P., O'Brien, T. P., Huston, S. L., Johnston, W. R., Guild, T. B., Friedel, R., et al. (2013). AE9, AP9 and SPM: New models for specifying the trapped energetic particle and space plasma environment. *Space Science Reviews*, *179*(1–4), 579–615. https://doi.org/10.1007/s11214-013-9964-y

Gross, B., West, J. E., von Seggern, H., & Berkley, D. A. (1980). Time-dependent radiation-induced conductivity in electron-irradiated teflon foils. *Journal of Applied Physics*, *51*(9), 4875–4881. https://doi.org/10.1063/1.328323

Gubby, R., & Evans, J. (2002). Space environment effects and satellite design. *Journal of Atmospheric and Solar-Terrestrial Physics*, *64*(16), 1723–1733. https://doi.org/10.1016/S1364-6826(02)00122-0

Han, J., Huang, J., Liu, Z., & Wang, S. (2005). Correlation of double star anomalies with space environment. *Journal of Spacecraft and Rockets*, *42*(6), 1061–1065. https://doi.org/10.2514/1.14773

Hands, A. D. P., Ryden, K. A., Sandberg, I., Heynderickx, D., Provatas, G., Animalragia-Giamini, S., et al. (2020). An update to MOBE-DIC using current monitor measurements from Galileo. *IEEE Transactions on Nuclear Science*, *67*(1), 181–190. https://doi.org/10.1109/TNS.2019.2944699

Hands, A. D. P., Ryden, K. A., Underwood, C., Rodgers, D., & Evans, H. (2015). A new model of outer belt electrons for dielectric internal charging (MOBE-DIC). *IEEE Transactions on Nuclear Science*, *62*(6), 2767–2775. https://doi.org/10.1109/TNS.2015.2475134

Hapgood, M., Angling, M. J., Attrill, G., Bisi, M., Cannon, P. S., Dyer, C., et al. (2021). Development of space weather reasonable worst-case scenarios for the UK national risk assessment. *Space Weather*, *19*(4), e2020SW002593. https://doi.org/10.1029/2020SW002593

Hastings, D., & Garrett, H. (2004). *Spacecraft-environment interactions*. Cambridge University Press.

Horne, R. B., Glauert, S. A., Kirsch, P., Heynderickx, D., Bingham, S., Thorn, P., et al. (2021). The satellite risk prediction and radiation forecast system (SaRIF). *Space Weather*, *19*(12), e2021SW002823. https://doi.org/10.1029/2021SW002823

Horne, R. B., Meredith, N. P., Thorne, R. M., Heynderickx, D., Iles, R. H. A., & Anderson, R. R. (2003). Evolution of energetic electron pitch angle distributions during storm time electron acceleration to megaelectronvolt energies. *Journal of Geophysical Research*, *108*(A1), SMP-11. https://doi.org/10.1029/2001JA009165

Horne, R. B., Phillips, M. W., Glauert, S. A., Meredith, N. P., Hands, A. D. P., Ryden, K., & Li, W. (2018). Realistic worst case for a severe space weather event driven by a fast solar wind stream. *Space Weather*, *16*(9), 1202–1215. https://doi.org/10.1029/2018SW001948

Horne, R. B., Thorne, R. M., Glauert, S. A., Albert, J. M., Meredith, N. P., & Anderson, R. R. (2005). Timescale for radiation belt electron acceleration by whistler mode chorus waves. *Journal of Geophysical Research*, *110*(A3), A03225. https://doi.org/10.1029/2004JA010811

Horne, R. B., Thorne, R. M., Shprits, Y. Y., Meredith, N. P., Glauert, S. A., Smith, A. J., et al. (2005). Wave acceleration of electrons in the Van Allen radiation belts. *Nature*, *437*(7056), 227–230. https://doi.org/10.1038/nature03939

Iucci, N., Levitin, A. E., Belov, A. V., Eroshenko, E. A., Ptitsyna, N. G., Villoresi, G., et al. (2005). Space weather conditions and spacecraft anomalies in different orbits. *Space Weather*, *3*(1), S01001. https://doi.org/10.1029/2003SW000056

Kennel, C. F., & Petschek, H. E. (1966). Limit on stably trapped particle fluxes. *Journal of Geophysical Research*, *71*, 1–28. https://doi.org/10.1029/JZ071i001p00001

Khatipov, S. A. (2001). Radiation-induced electron transport processes in polymeric dielectrics (a review). *High Energy Chemistry*, *35*(5), 291–307. https://doi.org/10.1023/A:1011914004155

Koons, H. C. (2001). Statistical analysis of extreme values in space science. *Journal of Geophysical Research*, *106*(A6), 10915–10921. https://doi.org/10.1029/2000JA000234

Lam, P. Y., Horne, R. B., Meredith, N. P., Glauert, S. A., & Kirsch, P. (2024). Charging currents and electric fields of satellite cables during a reasonable worst case scenario (Version 1.0) [Dataset]. *NERC EDS UK Polar Data Centre*. https://doi.org/10.5285/3948ce45-3430-468d-8e99-22d4d6c0a8c5

Mauk, B. H., & Fox, N. J. (2010). Electron radiation belts of the solar system. *Journal of Geophysical Research*, *115*(A12), A12220. https://doi.org/10.1029/2010JA015660

Meredith, N. P., Cayton, T. E., Cayton, M. D., & Horne, R. B. (2023). Extreme relativistic electron fluxes in GPS orbit: Analysis of NS41 BDD-IIR data. *Space Weather*, *21*(6), e2023SW003436. https://doi.org/10.1029/2023SW003436

Meredith, N. P., Horne, R. B., Isles, J. D., & Green, J. C. (2016). Extreme energetic electron fluxes in low Earth orbit: Analysis of POES $e > 30$, $e > 100$, and $e > 300$ keV electrons. *Space Weather*, *14*(2), 136–150. https://doi.org/10.1002/2015SW001348

Meredith, N. P., Horne, R. B., Isles, J. D., & Rodriguez, J. V. (2015). Extreme relativistic electron fluxes at geosynchronous orbit: Analysis of goes $e > 2$ MeV electrons. *Space Weather*, *13*(3), 170–184. https://doi.org/10.1002/2014SW001143

Meredith, N. P., Horne, R. B., Isles, J. D., Ryden, K. A., Hands, A. D. P., & Heynderickx, D. (2016). Extreme internal charging currents in medium Earth orbit: Analysis of SURF plate currents on Giove-A. *Space Weather*, *14*(8), 578–591. https://doi.org/10.1002/2016SW001404

Morley, S. K., Sullivan, J. P., Henderson, M. G., Blake, J. B., & Baker, D. N. (2016). The Global Positioning System constellation as a space weather monitor: Comparison of electron measurements with Van Allen Probes data,. *Space Weather*, *14*(2), 76–92. https://doi.org/10.1002/2015SW001339

NASA. (2022). Mitigating in-space charging effects—A guideline, NASA technical handbook, NASA-HDBK-4002B, National Aeronautics and space administration. In *USA. NASA technical handbook*.

O'Brien, T. P., Fennell, J. F., Roeder, J. L., & Reeves, G. D. (2007). Extreme electron fluxes in the outer zone. *Space Weather*, *5*(1), S01001. https://doi.org/10.1029/2006SW000240

Olifer, L., Mann, I. R., Claudepierre, S. G., Baker, D. N., Spence, H. E., & Ozeke, L. G. (2022). A natural limit to the spectral hardness of worst case electron radiation in the terrestrial Van Allen belt. *Journal of Geophysical Research: Space Physics*, *127*(8), e2022JA030506. https://doi.org/10.1029/2022JA030506

Olifer, L., Mann, I. R., Kale, A., Mauk, B. H., Claudepierre, S. G., Baker, D. N., et al. (2021). A tale of two radiation belts: The energy-dependence of self-limiting electron space radiation. *Geophysical Research Letters*, *48*(20), e2021GL095779. https://doi.org/10.1029/2021GL095779

Olson, W. P., & Pfitzer, K. (1977). Magnetospheric magnetic field modeling. In *Annual scientific report, AFOSAR contract no. F44620-75-c-0033*.

Paulmier, T., Dirassen, B., Arnaout, M., Payan, D., & Balcon, N. (2015). Radiation-induced conductivity of space used polymers under high energy electron irradiation. *IEEE Transactions on Plasma Science*, *43*(9), 2907–2914. https://doi.org/10.1109/TPS.2015.2452943

Rodgers, D. J., Ryden, K. A., Wrenn, G. L., Latham, P. M., Sorensen, J., & Levy, L. (2000). An engineering tool for the prediction of internal dielectric charging. In *Proceedings of the 6th spacecraft charging conference, November 2–6, 1998* (pp. 125–130). AFRL Science Center. Retrieved from https://articles.adsabs.harvard.edu/pdf/1998sct..conf..125R

Rodgers, D. J., Ryden, K. A., Wrenn, G. L., Levy, L., & Sorensen, J. (2003). Fitting of material parameters for DICTAT internal dielectric charging simulations using DICFIT. In *Proceedings of the 9th international symposium on materials in a space environment, 16–20 June 2003* (pp. 609–613). ESA SP 540. Retrieved from http://esmat.esa.int/Materials_News/SP-540/papers/p3_rodge.pdf

Shi, R., Summers, D., Ni, B., Fennell, J. F., Blake, J. B., Spence, H. E., & Reeves, G. D. (2016). Survey of radiation belt energetic electron pitch angle distributions based on the Van Allen Probes MagEIS measurements. *Journal of Geophysical Research: Space Physics*, *121*(2), 1078–1090. https://doi.org/10.1002/2015JA021724

Tsurutani, B. T., Gonzalez, W. D., Lakhina, G. S., & Alex, S. (2003). The extreme magnetic storm of 1–2 September 1859. *Journal of Geophysical Research*, *108*(A7), 1268. https://doi.org/10.1029/2002JA009504

UKSSWPS. (2001). UK severe space weather preparedness strategy. Department for business. In *Energy and industrial strategy* (pp. 1–39). Retrieved from https://www.gov.uk/government/publications/uk-severe-space-weather-preparedness-strategy

Wrenn, G. L. (1995). Conclusive evidence for internal dielectric charging anomalies on geosynchronous communications spacecraft. *Journal of Spacecraft and Rockets*, *32*(3), 514–520. https://doi.org/10.2514/3.26645

Wrenn, G. L., Rodgers, D. J., & Buehler, P. (2000). Modeling the outer belt enhancements of penetrating electrons. *Journal of Spacecraft and Rockets*, *37*(3), 408–415. https://doi.org/10.2514/2.3575

Wrenn, G. L., Rodgers, D. J., & Ryden, K. A. (2002). A solar cycle of spacecraft anomalies due to internal charging. *Annales Geophysicae*, *20*(7), 953–956. https://doi.org/10.5194/angeo-20-953-2002